Journal of Alloys and Compounds 499 (2010) 231–237

Contents lists available at ScienceDirect

Journal of Alloys and Compounds

journal homepage: www.elsevier.com/locate/jallcom

Effect of pH on ZnO nanoparticle properties synthesized by sol–gel centrifugation

S.S. Alias, A.B. Ismail, A.A. Mohamad*

School of Materials and Mineral Resources Engineering, Universiti Sains Malaysia, 14300 Nibong Tebal, Penang, Malaysia

ARTICLE INFO

Article history:
Received 20 January 2010
Received in revised form 12 March 2010
Accepted 18 March 2010
Available online 25 March 2010

Keywords:
Sol–gel method
pH
Growth mechanism
Crystallite size
Particle size

ABSTRACT

ZnO nanoparticles were synthesized at different pH values by the sol–gel method and centrifuged at 3000 rpm for 30 min. The ZnO powders agglomerate when synthesized in acidic and neutral conditions (pH 6 and 7). Fine powders were obtained when the pH of the sols was increased to 9. The maximum crystallite size (25.36 nm) of the ZnO powder was obtained at pH 9. The particles sizes of the ZnO synthesized between pH 6 and 11 were in the range of 36.65–49.98 nm. Ultraviolet–visible analysis (UV–vis) also demonstrated that ZnO synthesized from pH 8 to 11 has good optical properties with band gap energy (E_g) between 3.14 and 3.25 eV.

1. Introduction

Zinc oxide (ZnO) has recently attracted significant interest for both fundamental studies and technical applications. In the past few years, ZnO has been synthesized using electrochemical deposition [1], chemical vapor deposition [2], catalysis-driven molecular beam epitaxy [3], thermal evaporation [4], pulsed laser deposition [5], zinc–air [6] and solution–gelation (sol–gel) [7]. Sol–gel is one of the most commonly selected methods for the synthesis of ZnO nanoparticles [8–10] because this method produces good homogeneity and optical properties and has easy composition control, low processing temperatures, the ability to coat large areas, and low equipment costs.

The sol pH is one of the important factors influencing the ZnO properties when ZnO is synthesized by sol–gel. The pH affects the hydrolysis and condensation behavior of the solution during gel formation and therefore influences the morphology of the ZnO [11]. For instance, Li et al. [12] showed that the solution conditions have a particular effect on ZnO particle-size powders. The pH can also change the number of ZnO nuclei and growth units [13]. Sagar et al. [14] claimed that the increase in pH (from acidic to alkaline) of the sols results in the growth of a ZnO film.

Metal alkoxides are often used as raw materials for the sol–gel process. In early work on the sol–gel method, an n-ZnO/p-Si heterojunction was prepared by the sol–gel process using zinc diethoxide as a starting material for synthesizing the ZnO films [15]. In the sol–gel method, the nucleation of the metal oxide particles occurs by precipitation. This precipitation involves a reaction between the soluble metal salt and the hydroxide ions or water. The nucleation reaction of a divalent metal salt (MX_2) and a solution containing hydroxide ions (YOH) can be describes as follows [16]:

$$MX_2 + 2YOH \rightarrow MO(s) + 2Y^+ + 2X^- + H_2O \quad (1)$$

where X is an anion ($CH_3CO_2^-$, Br^-, ClO_4^-) and Y is a cation (Na^+, Li^+, K^+).

ZnO nanoparticles can also be synthesized using divalent metal salts and an aqueous solution based on Eq. (1). Centrifuging is commonly used to separate species of different size, mass, or density. The mixture with denser components will migrate away from the axis of the centrifuge, and the less-dense components will migrate toward the axis. The Coriolis force influences crystal growth, and well-defined size characteristics can be generated by this processing method [17]. The goal of this work is to synthesis ZnO in aqueous solution with pH values ranging from 6 (acidic) to 11 (alkaline). The pH of the sol was controlled by a zinc acetate dihydrate [$Zn(CH_3COO)_2{\cdot}2H_2O$] precursor, and sodium hydroxide (NaOH) was used to control the aqueous pH. Centrifugation was used to improve the ZnO properties.

2. Experimental

2.1. Synthesis of ZnO powder

The ZnO sols were prepared by adding 0.2 M $Zn(CH_3COO)_2{\cdot}2H_2O$ (Sigma–Aldrich) to methanol (CH_3OH, Merck) at room temperature. The solution was stirred for 2 h using a magnetic stirrer until a clear solution without turbidity was obtained. The pH of the sols was ~5. The clear solution transformed into a milky white slurry solution after titration with 1.0 M NaOH (Merck). The

* Corresponding author. Tel.: +60 4599 6118; fax: +60 4594 1011.
E-mail addresses: azmin@eng.usm.my, azmin@hotmail.com (A.A. Mohamad).

0925-8388/$ – see front matter © 2010 Elsevier B.V. All rights reserved.
doi:10.1016/j.jallcom.2010.03.174

addition of NaOH changed the pH values of the sol from 6 (acidic condition) to 11 (alkaline condition). The resulting milky white gel was stirred for another 1 h. All of the samples were left alone for 1 week to allow the sol–gel process to finish.

After 1 week, the sols were centrifuged using a Rotina 38 at 3000 rpm for 30 min to complete gelation and hydrolysis. Next, the wet, white precipitate of ZnO was removed from the centrifuge and dried at 80 °C for 1 h. Finally, the dried precipitate was ground to a fine white powder.

2.2. Characterization of ZnO powder

The structure of the synthesized ZnO powder was studied using X-ray diffraction (XRD, Bruker Advanced X-ray Solutions D8). The XRD results obtained were compared to the Joint Committee on Powder Diffraction Standards (JCPDS) X-ray data file. The crystallite size of the samples was obtained by measuring the broadening of the XRD peaks with preferred orientation and using the Scherrer formula:

$$LC = \frac{180}{\pi} \cdot \frac{\kappa \cdot \lambda}{\cos\theta \cdot \sqrt{\mathrm{FWHM}^2 - s^2}} \quad (2)$$

where $\pi = 3.142$, λ is the wavelength of Cu K_α radiation (1.5406 Å), κ is the Scherrer constant (0.89), s is the instrumental broadening (0), FWHM is the full-width at half-maximum of the (1 0 1) plane, and θ is the angle corresponding to the (1 0 1) plane. The FWHM and θ were taken directly from the *EVA* software that was provided with the XRD analysis.

The surface morphology, particles size and composition of ZnO nanoparticles were investigated by field emission scanning electron microscopy (FESEM) and energy dispersive X-ray spectroscopy (EDX, Zeiss Supra 35VP). The FTIR analysis was performed in order to determine the functional group of materials existed in all ZnO samples. The analysis was recorded using FTIR spectrometer (Perkin-Elmer®) in a range between 4000 and 400 cm^{-1}. The optical properties and band gap energies of ZnO nanoparticles were analyzed using Ultraviolet–visible (UV–vis) spectroscopy (Perkin-Elmer Lambda 35). The absorbance as a function of band gap energy (E_g) of ZnO powder synthesized at pH 8–11 was plotted from UV–vis analysis.

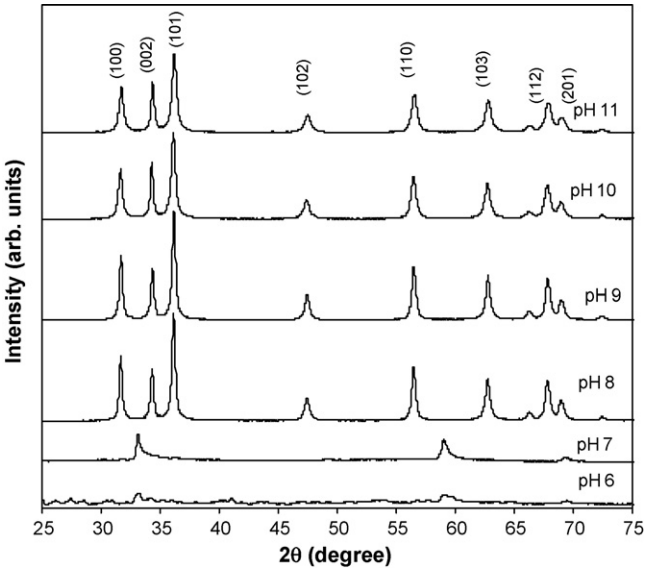

Fig. 1. XRD of ZnO synthesized via the sol–gel method at various pH values.

The absorbance values can be determined directly from UV–vis spectra analysis and $h\nu$ was calculated by using wavelength (λ) value since $h\nu = (h \times c)/\lambda$, where h = Planck constant (6.62×10^{-34}), c = speed of light (3×10^8 m s^{-1}) and λ = value of wavelength (between 600 and 300 nm). The E_g value was determined by extrapolating the linear portion of the E_g axis curve to zero absorbance.

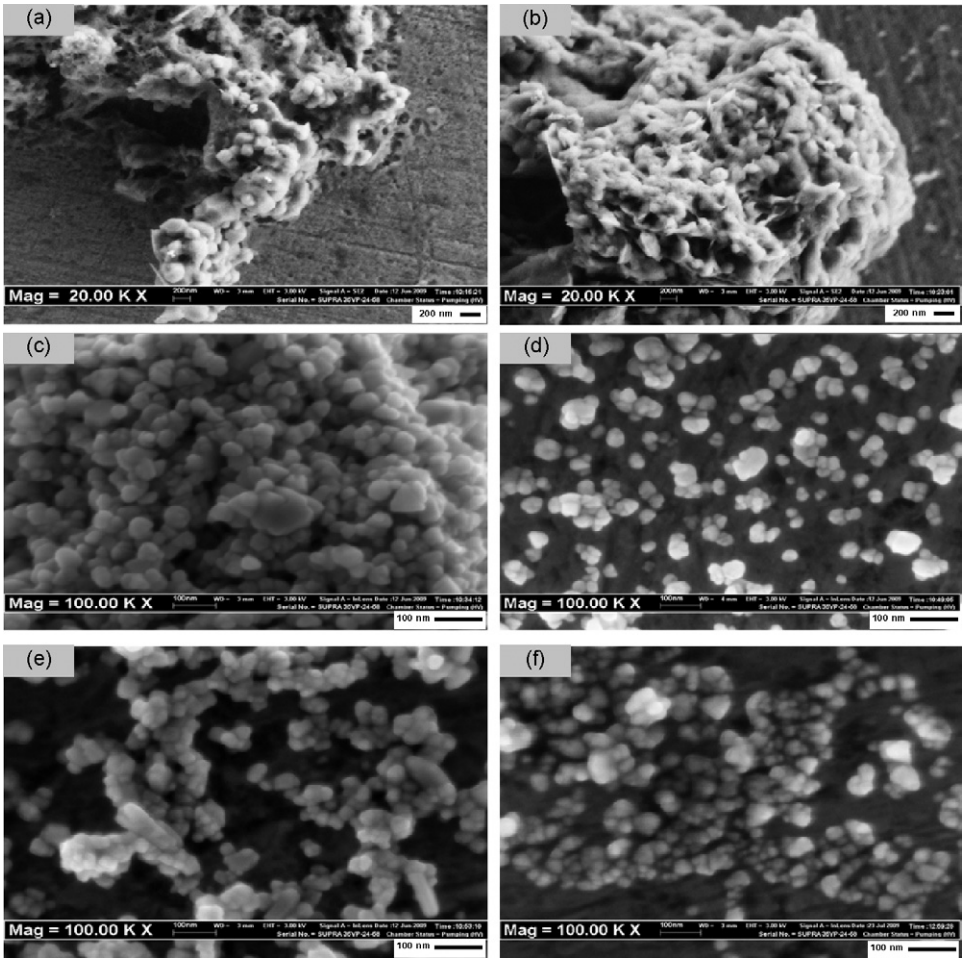

Fig. 2. FESEM of ZnO powder synthesized at various pH values: (a) pH 6, (b) pH 7, (c) pH 8, (d) pH 9, (e) pH 10 and (f) pH 11.

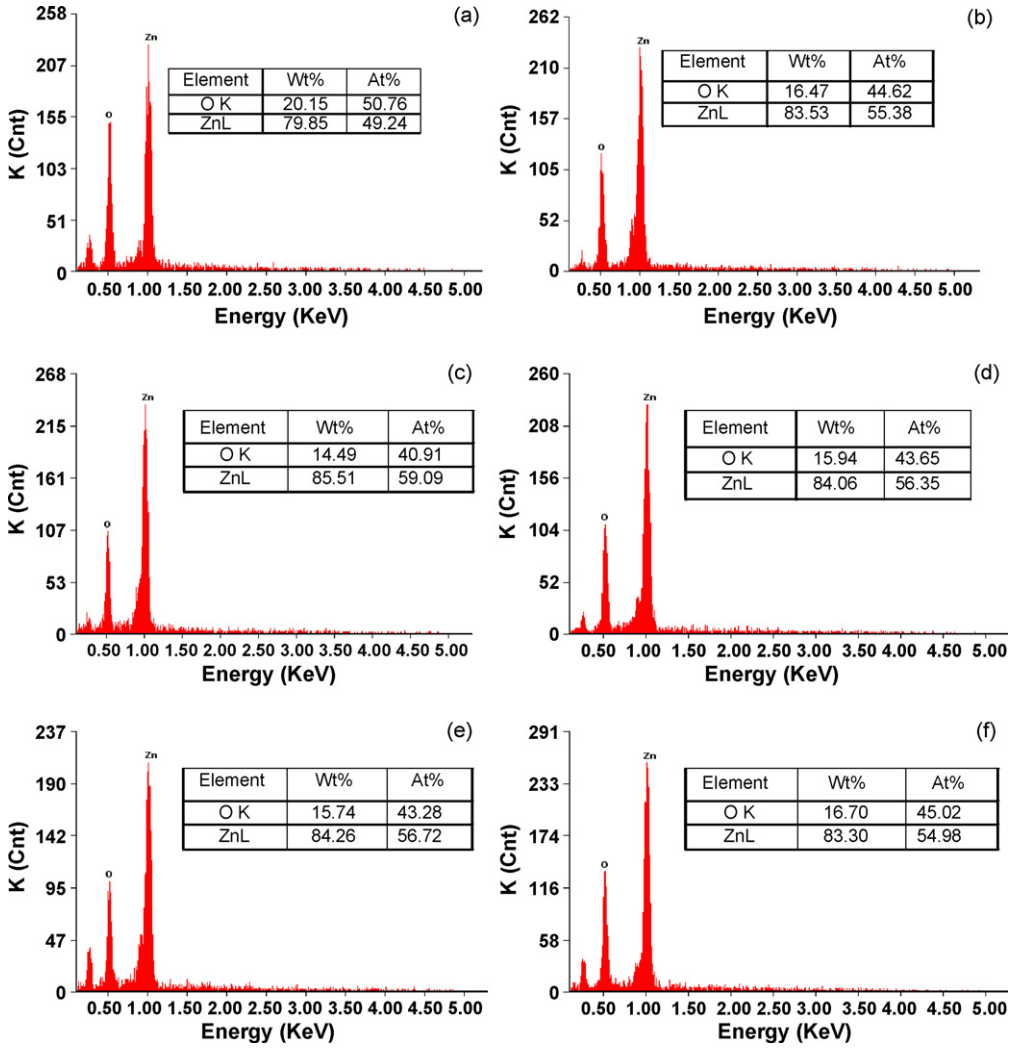

Fig. 3. EDX of ZnO powder synthesized at various pH values: (a) pH 6, (b) pH 7, (c) pH 8, (d) pH 9, (e) pH 10 and (f) pH 11.

3. Results and discussion

3.1. X-ray diffraction analysis

Fig. 1 shows the XRD profiles of ZnO powders prepared pH values of 6, 7, 8, 9, 10 and 11. The samples prepared at pH 6 and 7 have no intense ZnO peak. Normally, the ZnO structure cannot be synthesized well at pH 6 because of the high concentration of H^+ ions and low concentration of OH^- ions in the sol. For the neutral condition at pH 7, the number of H^+ ions reacting with number of OH^- from NaOH is equivalent. Therefore, both of the peaks are broad. The ZnO powder peaks for samples with pH ≥ 8 show the crystalline nature with angles of diffraction (2θ) = 31.68°, 34.35°, 36.16°, 47.45°, 56.48°, 62.74°, 67.84° and 68.96°. The three most intense peaks correspond to the (1 0 0), (0 0 2) and (1 0 1) planes. The preferred orientation corresponding to the (1 0 1) plane is observed for ZnO powder with pH ≥ 8. The highest ZnO intensity peak (2θ = 36.16°) appears at pH 9 because a sufficient amount of OH^- is available to form ZnO.

The observed peaks intensity patterns can be attributed to the presence of a hexagonal wurtzite structure in the ZnO powder. The cell constants are c = 5.205 Å and a = 3.249 Å. These values and the wurtzite structure are confirmed by the JCPDS 36-1451 data. No other peaks were detected for samples at pH ≥ 8, indicating that all of the precursors were completely decomposed and no other complex products were formed. The XRD results confirm that the powders synthesized in this work are ZnO. This result is similar to results achieved by others [18–20].

3.2. Surface morphology and composition

FESEM images of ZnO powder nanoparticles are shown in Fig. 2. Large bulk particles with high agglomeration are shown in Fig. 2a and b. This agglomeration is a result of the acidic and neutral pHs of the $Zn(OH)_2$ sols during the synthesis process. Both samples lack sufficient OH^- ions. Fig. 2c and d shows that the particles are homogeneous with a good nanostructure when the pH is increased to alkaline conditions (pH 8 and 9). ZnO nanoparticles are mostly spherical in shape. A powder of ZnO nanoparticles with low agglomeration was obtained in this work. This low agglomeration is attributed to the use of a centrifuge instead of the traditional sol–gel method, which does not include centrifuge processing [21]. Centrifugation can remove impurities such as $Zn(OH)_2$ by enhancing the interaction between Zn–O and the solvent.

The OH^- ions allow the nucleation and growth of ZnO and the formation of particles. Particles sizes decrease (Fig. 2e and f) when the pH of the sols is above 9. Wu et al. [22] claim that the large particles consist of agglomerated nanoparticles and that either compact or porous polycrystalline micron-sized particles can be formed using colloidal sol–gel technique. In this work, the sizes of the par-

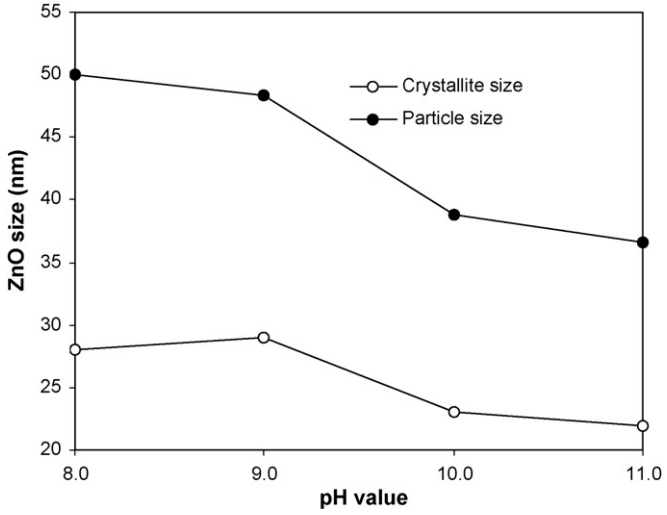

Fig. 4. Crystallite and particle sizes of ZnO synthesized at various pH.

ticles at lower pH values are nano-sized even when agglomeration still occurs. Average particle of ZnO synthesized at a pH between 9 and 11 are uniform in size with and range between 36.65 and 49.98 nm in diameter. The chemical composition of the ZnO powder synthesized at pHs between 6 and 11 were studied using EDX (Fig. 3a–f). The existence of impurities peaks near origin *X*-axis due to C and O are contributed by methanol solvent. The ZnO powders initially dispersed in methanol before FESEM and EDX analysis.

The atomic percentages of Zn and O are close to the stoichiometric composition and have a ratio of approximately 1:1. This result confirms that the powder contains only Zn and O elements.

3.3. Comparison between crystallite and particle size

The crystallite and particle sizes of the ZnO powder are plotted as a function of pH in Fig. 4. The crystallite size of ZnO ranges from 18.37 to 25.36 nm. The largest crystallite size (25.36 nm) occurs at pH 9, and the smallest size (18.37 nm) occurs at pH 11. The particle size is large compare to crystallite size. The particle size ranged from 36.65 to 49.98 nm, ~25 nm larger than the crystallite size. Particle-size analysis reveals that the largest particle size (49.98 nm) occurs at pH 8, and the smallest particle size (36.65 nm) occurs at pH 11. The crystallite and particle sizes are inversely proportional to the pH values. The sizes of the ZnO powder crystallites and particles are tabulated in Table 1.

Table 1
Comparison between crystallite and particle size of ZnO synthesized at various pH values.

pH	Crystallite size (nm)	Particle size (nm)
8	24.96	49.98
9	25.36	48.31
10	21.87	38.32
11	18.37	36.65

Because ZnO is absent from the XRD results, the crystallite and particle size of ZnO synthesized at pH 6 and 7 cannot be calculated. Further increasing the concentration of OH^- from pH 9 reduces the ZnO crystallite and particle sizes because the amount of dissolved OH^- was larger during synthesis of ZnO at pH > 9. When ZnO reacts with too much OH^-, the dissolution of ZnO occurs [23]. The dissolution made the crystallites and particles became smaller and agglomerated.

3.4. FTIR analysis of ZnO

Fig. 5 shows the FTIR spectra of ZnO synthesized at various pH values. The bands at 3543–3393 cm^{-1} in Region 1 correspond to the O–H mode of vibration [24]. The broad O–H peaks become more narrow with an increase in the pH value because the additional amount of O–H from the NaOH reacts with the $Zn(CH_3COO)_2{\cdot}2H_2O$ at pH values ≥8. The strong asymmetric stretching mode of vibration of C=O was observed between 1612 and 1560 cm^{-1} in Region 2. The symmetric stretching occurs between 1453 and 1333 cm^{-1} because of the presence of C–O. Both of these peaks are shifted inconsistently because of diverging structural morphologies in alkaline conditions [25]. The C–O–C peak is present between 1023 and 1020 cm^{-1}. According to Du et al. [26], the

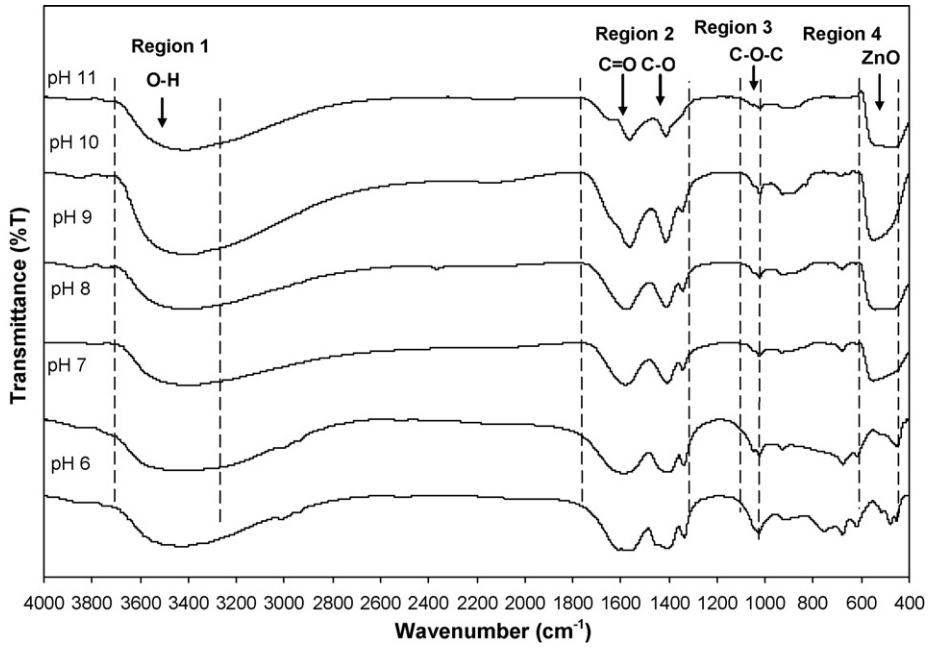

Fig. 5. FTIR spectra of ZnO synthesized at various pH values.

Table 2
FTIR of ZnO at various pH values.

pH	Wavenumber (cm^{-1})	Functional group
6	3543	O–H
	1612–1584,1453–1333	C=O, C–O
	1023–1020	C–O–C
	515–453	ZnO
7	3411	O–H
	1585, 1404–1340	C=O, C–O
	1023–1020	C–O–C
	453	ZnO
8	3393	O–H
	1579, 1407–1341	C=O, C–O
	1023–1020	C–O–C
	457	ZnO
9	3392	O–H
	1579, 1411–1341	C=O, C–O
	1023–1020	C–O–C
	543	ZnO
10	3400	O–H
	1560, 1412–1346	C=O, C–O
	1023–1020	C–O–C
	550	ZnO
11	3393	O–H
	1560, 1412	C=O, C–O
	1023–1020	C–O–C
	550	ZnO

C–O–C peak usually appears at 1256 cm^{-1}. The existence of other peaks instead of ZnO and O–H which are C=O, C–O, C–O–C group from $Zn(CH_3COO)_2{\cdot}2H_2O$ precursor, CH_3OH solvent are not much affected on the synthesized of ZnO powders. The FTIR analysis wavenumber results in Table 2 proved this statement. These three functional groups wave numbers not much have different when increasing pH values compare to the O–H and ZnO groups. In fact the XRD and EDX analysis proved that the synthesized powders in this work are ZnO with the good stoichiometric composition.

The particle size caused a large shift in the IR peak. The ZnO peak that appears in the range of 550–453 cm^{-1} shows that the transformation of $Zn(OH)_2$ to ZnO was completed. Previous researches found the ZnO peak between 464 and 419 cm^{-1} [18,27,28]. In this study, the ZnO peaks of all samples were shifted inconsistently because of the effect of ZnO particles sizes changing with pH [29]. Thus, the particle-size affects the peak shifts. The FTIR results support the FESEM results.

3.5. Mechanism of ZnO growth

The growth mechanism of the powder of ZnO nanoparticles during the sol–gel process as described in Eqs. (4)–(7) is shown in Fig. 6. Sol–gel formation can be divided into four steps: (i) hydrolysis, (ii) condensation and polymerization (nucleation) of monomers to form particles, (iii) growth of particles and (iv) aging. To grow ZnO with high crystallinity, a sufficient amount of OH^- is needed to dissolve the ZnO. At pH ≥ 8.0, $Zn(OH)_4^{2-}$ is converted to ZnO because of the high chemical potential of OH^- at equilibrium with a dehydration reaction [30]:

$$OH^- + OH^- \rightarrow O^{2-} + H_2O \quad (4)$$

To allow condensation to occur, the zero-charge precursor molecules $Zn(CH_3COO)_2{\cdot}2H_2O$ (Fig. 6a) need to be formed with a specific amount of water or NaOH. During the initial stage of the reaction, the aqueous solution of $Zn(CH_3COO)_2{\cdot}2H_2O$ reacts with NaOH to form zinc hydroxide [$Zn(OH)_2$], sodium acetate (CH_3COONa) and water molecules [10]. This transformation can be

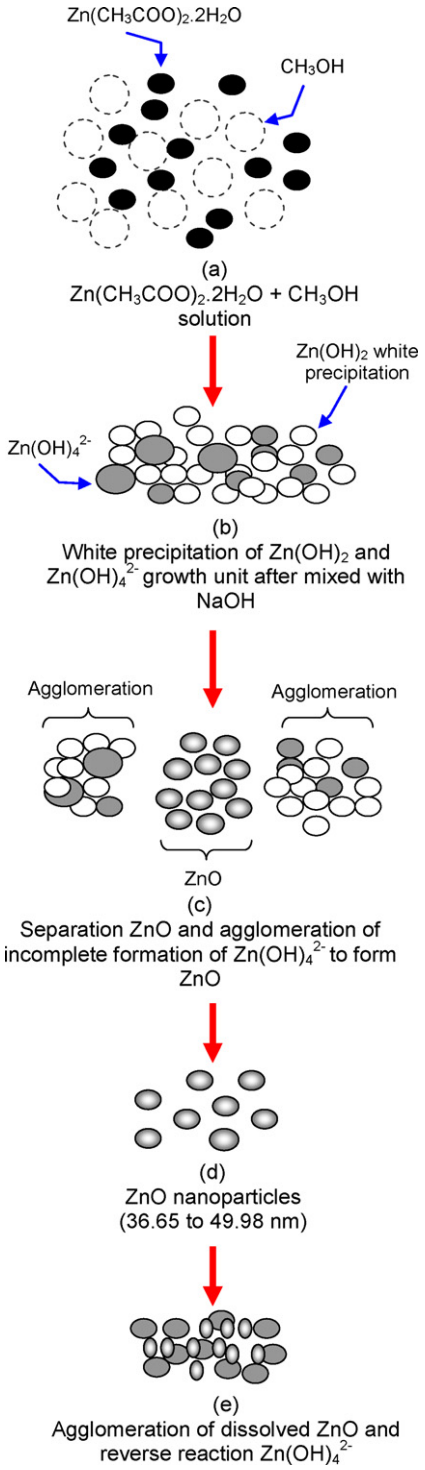

Fig. 6. Schematic illustration of the growth mechanism of ZnO nanoparticles.

represented by the following chemical reaction [26,31]:

$$Zn(CH_3COO)_2{\cdot}2H_2O + 2NaOH \rightarrow Zn(OH)_2 + 2CH_3COONa + 2H_2O \quad (5)$$

The build-up of precursor molecules results in a supersaturation of the solution (Fig. 6b). Nucleation occurs continuously above and below the condensation and polymerization threshold. The $Zn(OH)_2$ reacts with the water molecule to form the growth unit

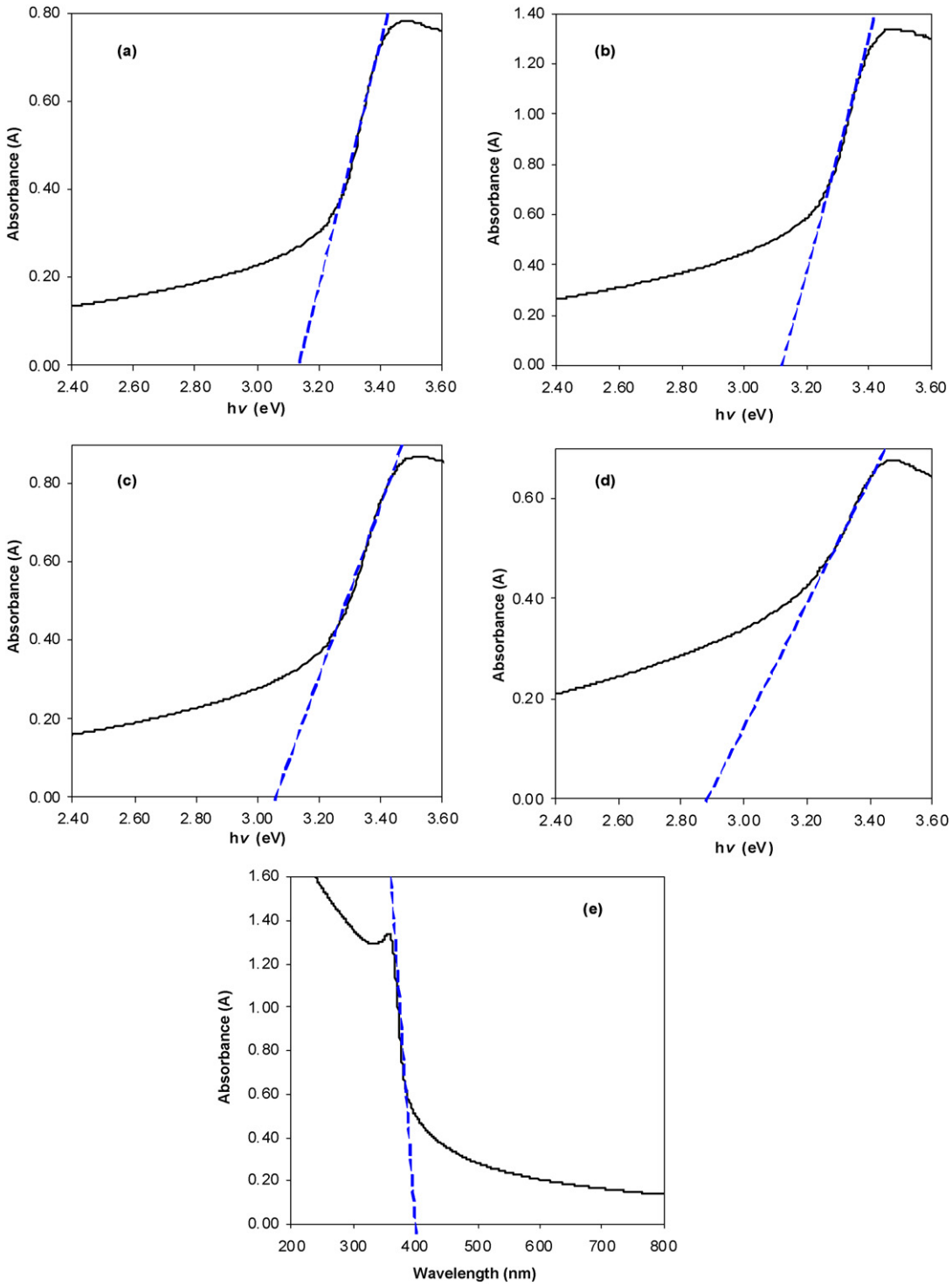

Fig. 7. UV–vis analysis of ZnO powder from pH 8 to 11: (a) pH 8, (b) pH 9, (c) pH 10, (d) pH 11 and (e) pH 9 (as a function of wavelength).

$Zn(OH)_4^{2-}$ and hydrogen ions ($2H^+$) as follows:

$$Zn(OH)_2 + 2H_2O \rightarrow Zn(OH)_4^{2-} + 2H^+ \quad (6)$$

Fig. 6c shows that further growth of ZnO and separation of agglomerates from the supersaturated solution is possible until the solution becomes saturated with a white precipitate of colloidal-gel $Zn(OH)_4^{2-}$. Centrifugation transforms the $Zn(OH)_4^{2-}$ into ZnO according to the following reaction [32]:

$$Zn(OH)_4^{2-} \rightarrow ZnO + H_2O + 2OH^- \quad (7)$$

Oskam [10] states that the two dominant processes that take place during aging are aggregation and coarsening. In this work, the aging rates of nanoparticles depend strongly on the pH values. This parameter determines the structure and size distribution of the final spherical nanoparticles (Fig. 6d). Centrifugation removes the agglomeration of incompletely transformed $Zn(OH)_4^{2-}$ and spins this $Zn(OH)_4^{2-}$ to allow a complete transformation to ZnO.

However, at higher OH^- concentrations i.e. at pH 10 and 11, ZnO reacts with OH^-. This dissolution of ZnO during reverse reaction

Table 3
Energy gap of ZnO at different pH values.

pH	Energy gap, E_g (eV)
8	3.25
9	3.24
10	3.23
11	3.14

produce $Zn(OH)_4^{2-}$ according to this reaction [23]:

$$ZnO + H_2O + 2OH^- \rightarrow Zn(OH)_4^{2-} \quad (8)$$

Dissolution of larger ZnO produced small ZnO particles. Meanwhile combination of these small particle and $Zn(OH)_4^{2-}$ produce an agglomeration (Fig. 6e). Centrifugation also accelerated this reaction.

3.6. ZnO optical properties

The plot of absorbance as a function of band gap energy (E_g) of ZnO powder synthesized at pH 8–11 is illustrated in Fig. 7a–d. The E_g value for ZnO at pH 6 and 7 are not shown because the particles are large in size and agglomerate. By extrapolating the linear portion of the curve to zero absorbance, the direct band gap energy of the synthesized powder from pH 8 to 11 was found to be in the range of 2.86–3.14 eV. These E_g values are similar to results obtained in previous studies [33,34]. The ZnO sample at pH 9 has the highest absorbance curve in the UV region of 3.14 eV. The optical absorbance of ZnO as a function of wavelength for ZnO at pH 9 is shown in Fig. 7e. The sharp decrease in intensity of transmitted light around 400 nm is a result of band edge absorption [35]. This shift tendency mainly relates to the confinement effect of the small size of ZnO [36].

The details of E_g at different pH values are shown in Table 3. The level of optical absorption strongly depends on particles size. The E_g values decrease with decreasing particle size. As stated in Section 3.3, the particles size decreases as the pH increases. Consequently, the size of the particles influences the ability of ZnO nanoparticles to absorb UV light.

The most relevant parameter for the application of ZnO to opto-electronics is the large E_g, which varies from 3.0 to 3.4 eV at room temperature [37]. For example, Rao and Dutta [38] obtained the conversion efficiency of 4.7% for ZnO dye-sensitized solar cell (DSSC). In addition, ZnO with E_g value 3.2 eV have been used as working electrode for DSSC and recognized as potential material to substitute TiO_2 based DSSC working electrode [39]. The UV–vis results support all of the ZnO powder characterization analysis. The diverse characterizations of ZnO at different pH values influence its properties.

4. Conclusion

ZnO nanoparticles powders have been successfully synthesized by the sol–gel technique at different pH values using centrifugation. All of the samples have good structural, morphological and optical properties. ZnO synthesized at pH 9 has the best properties. At pH 9, the ZnO has an average particles size of about 48.31 nm, and the particles are nearly uniform and spherical. The influence of nanocrystallinity can be seen in the band gap enhancement of 3.24 eV.

Acknowledgements

SSA would like to thank MOSTI for the National Science Fellowship award and USM-RU-PRGS for Grant (8031020). AAM wish to thanks USM Short Term Grant (6039030) for their financial support in this study.

References

[1] S. Peulon, D. Lincot, Adv. Mater. 8 (1996) 166–1166.
[2] J.-J. Wu, S.-C. Liu, J. Phys. Chem. B 106 (2002) 9546–9551.
[3] Y.W. Heo, V. Varadarajan, M. Kaufman, K. Kim, D.P. Norton, F. Ren, P.H. Fleming, Appl. Phys. Lett. 81 (2002) 3046–3048.
[4] B.D. Yao, Y.F. Chan, N. Wang, Appl. Phys. Lett. 81 (2002) 757–759.
[5] Y. Zhang, R.E. Russo, S.S. Mao, Appl. Phys. Lett. 87 (2005) 043106–43113.
[6] C.K. Yap, W.C. Tan, S.S. Alias, A.A. Mohamad, J. Alloys Compd. 484 (2009) 934–938.
[7] D. Sun, M. Wong, L. Sun, Y. Li, N. Miyatake, H.-J. Sue, J. Sol–Gel Sci. Technol. 43 (2007) 237–243.
[8] Z. Hu, G. Oskam, R.L. Penn, N. Pesika, P.C. Searson, J. Phys. Chem. B 107 (2003) 3124–3130.
[9] E.A. Meulenkamp, J. Phys. Chem. B 102 (1998) 5566–5572.
[10] G. Oskam, J. Sol–Gel Sci. Technol. 37 (2006) 161–164.
[11] R. Wahab, S.G. Ansari, Y.S. Kim, M. Song, H.-S. Shin, Appl. Surf. Sci. 255 (2009) 4891–4896.
[12] W.J. Li, E.W. Shi, T. Fukuda, Cryst. Res. Technol. 38 (2003) 847–858.
[13] H. Zhang, Xiangyang, Y. Ji, J. Xu, D. Que, D. Yang, Nanotechnology 15 (2004) 622–626.
[14] P. Sagar, P.K. Shishodia, R.M. Mehra, Appl. Surf. Sci. 253 (2007) 5419–5424.
[15] T. Okamura, Y. Seki, S. Nagakari, H. Okushi, Jpn. J. Appl. Phys. Part 1: Regul. Pap. Short Notes Rev. Pap. 31 (1992) 3218–3220.
[16] E.M. Wong, P.G. Hoertz, C.J. Liang, B.-M. Shi, G.J. Meyer, P.C. Searson, Langmuir 17 (2001) 8362–8367.
[17] D.J. Duval, B.J. McCoy, S.H. Risbud, Z.A. Munir, J. Appl. Phys. 83 (1998) 2301–2307.
[18] K. Anna, P. Nina, K. Yuri, M. Meinhard, Z. Werner, G. Aharon, Ultrason. Sonochem. 15 (2008) 839–845.
[19] U.N. Maiti, S.F. Ahmed, M.K. Mitra, K.K. Chattopadhyay, Mater. Res. Bull. 44 (2009) 134–139.
[20] M. Mazloumi, S. Taghavi, H. Arami, S. Zanganeh, A. Kajbafvala, M.R. Shayegh, S.K. Sadrnezhaad, J. Alloys Compd. 468 (2009) 303–307.
[21] S. Rani, P. Suri, P.K. Shishodia, R.M. Mehra, Sol. Energy Mater. Sol. Cells 92 (2008) 1639–1645.
[22] L. Wu, Y. Wu, Y. Lü, Mater. Res. Bull. 41 (2006) 128–133.
[23] N. Daneshvar, S. Aber, M.S. Seyed Dorraji, A.R. Khataee, M.H. Rasoulifard, Sep. Purif. Technol. 58 (2007) 91–98.
[24] D.M. Fernandes, R. Silva, A.A.W. Hechenleitner, E. Radovanovic, M.A.C. Melo, E.A.G. Pineda, Mater. Chem. Phys. 115 (2009) 110–115.
[25] H. Usui, J. Colloid Interface Sci. 336 (2009) 667–674.
[26] H. Du, F. Yuan, S. Huang, J. Li, Y. Zhu, Chem. Lett. 33 (2004) 770–771.
[27] H. Li, J. Wang, H. Liu, C. Yang, H. Xu, X. Li, H. Cui, Vacuum 77 (2004) 57–62.
[28] R. Wahab, S.G. Ansari, Y.-S. Kim, H.-K. Seo, H.-S. Shin, Appl. Surf. Sci. 253 (2007) 7622–7626.
[29] R. Wahab, S.G. Ansari, Y.S. Kim, M.A. Dar, H.-S. Shin, J. Alloys Compd. 461 (2008) 66–71.
[30] E. Hosono, S. Fujihara, T. Kimura, H. Imai, J. Sol–Gel Sci. Technol. 29 (2004) 71–79.
[31] W.J. Li, E.W. Shi, W.Z. Zhong, Z.W. Yin, J. Cryst. Growth 203 (1999) 186–196.
[32] N. Uekawa, R. Yamashita, Y.J. Wu, K. Kakegawa, Phys. Chem. Chem. Phys. 6 (2004) 442–446.
[33] R.E. Marotti, D.N. Guerra, C. Bello, G. Machado, E.A. Dalchiele, Sol. Energy Mater. Sol. Cells 82 (2004) 85–103.
[34] S. Monticone, R. Tufeu, A.V. Kanaev, J. Phys. Chem. B 102 (1998) 2854–2862.
[35] M.N. Kamalasanan, S. Chandra, Thin Solid Films 288 (1996) 112–115.
[36] C.-H. Hung, W.-T. Whang, Mater. Chem. Phys. 82 (2003) 705–710.
[37] S.J. Pearton, D.P. Norton, K. Ip, Y.W. Heo, T. Steiner, Prog. Mater. Sci. 50 (2005) 293–340.
[38] A.R. Rao, V. Dutta, Nanotechnology 19 (2008) 445712.
[39] G. Boschloo, T. Edvinsson, A. Hagfeldt (Eds.), Dye-sensitized Nanostructured ZnO Electrodes for Solar Cell Applications. Handbook of Nanostructured Materials for Solar Energy Conversion, T. Soga, Elsevier B.V., Amsterdam, 2006, pp. 227–254.